

Impact of Volcanic Aerosols on Stratospheric Ozone Recovery

Short/Running Title: Impact of volcanic aerosols on stratospheric ozone

Vaishali Naik¹, Larry W. Horowitz¹, M. Daniel Schwarzkopf¹, and Meiyun Lin^{1,2}

¹NOAA Geophysical Fluid Dynamics Laboratory, Princeton, NJ 08540

²Program in Atmospheric and Oceanic Sciences, Princeton University, Princeton, NJ 08540

Corresponding Author: V. Naik (Vaishali.Naik@noaa.gov)

Submitted on September 30, 2016.

Key Points:

- Elevated volcanic aerosol in the RCP4.5 and RCP8.5 scenarios lead to earlier ozone recovery.
- Volcanic aerosols contribute to uncertainty in stratospheric ozone recovery
- Projections of stratospheric ozone should consider volcanic aerosols

19 **Abstract**

20 We use transient chemistry-climate model simulations over the 2006-2100 time period to show
21 how the influence of volcanic aerosols on the extent and timing of ozone recovery varies with a)
22 future greenhouse gas scenarios (RCP4.5 and RCP8.5) and b) halogen loading. With background
23 aerosol loadings, global mean stratospheric ozone is simulated to return to 1980 levels around
24 2050 in the RCP8.5 scenario but remains below 1980 levels throughout the 21st century in the
25 RCP4.5 scenario. In contrast, with elevated volcanic aerosol loadings, ozone column recovers
26 more quickly to 1980 levels, with recovery dates ranging from the mid-2040s in RCP8.5 to the
27 mid-2050s to early 2070s in RCP4.5. The ozone response in both future emission scenarios is
28 greater for moderate compared with low volcanic aerosol loadings. These responses are
29 consistent with our current understanding of the influence of volcanic aerosols on ozone under
30 conditions of high and low halogen loadings. For the range of aerosol loadings considered here,
31 by 2100, the 1980-baseline adjusted global stratospheric ozone column is projected to be about
32 20-40% greater in RCP8.5 and 110-200% greater in RCP4.5 with elevated volcanic aerosols
33 compared to simulations with background aerosols. The ozone response to elevated volcanic
34 aerosols appears to be sensitive to the factor of 2.5 greater methane in RCP8.5 compared with
35 that in RCP4.5. Our results demonstrate the substantial uncertainties in stratospheric ozone
36 projections and expected recovery dates induced by volcanic aerosol perturbations that need to
37 be considered in future model ozone projections.

38 **1. Introduction**

39 Stratospheric aerosols affect stratospheric ozone directly by affecting heterogeneous
40 chemistry and photolysis rates and indirectly by influencing stratospheric temperature and large-
41 scale circulation patterns [*SPARC*, 2006]. Recent measurements indicate that there has been a
42 continuous increase in stratospheric aerosols over the last decade following a period (1998-2002)
43 of “background” (non-volcanic) aerosol levels. This increase has been attributed to a series of
44 moderate tropical volcanic eruptions [*Vernier et al.*, 2011]. However, the impact of volcanic
45 perturbations on the evolution of stratospheric ozone in the 21st century has not been considered
46 in projections of long term stratospheric ozone changes using chemistry-climate models [*Eyring*
47 *et al.*, 2010a, 2013]. For example, volcanic aerosols were set to zero or to near-zero background
48 in future climate projections conducted for the Coupled Model Intercomparison Project Phase 5
49 (CMIP5) [*Collins et al.*, 2014; see their Table 12.1]. Here we explore the evolution of
50 stratospheric ozone for the 2006-2100 time in response to two future climate forcing scenarios
51 under three different fixed levels of volcanic aerosol loading. We highlight the contrasting effects
52 of volcanic aerosol amounts under high (e.g., present-day) and low (e.g., future) halogen loading
53 (e.g., *Austin et al.* [2013]), the differing responses to greenhouse gas abundances, and resulting
54 influence on the timing of ozone recovery.

55 Volcanic eruptions enhance the background stratospheric aerosol layer, first identified by
56 *Junge et al.* [1961], by injecting large amounts of sulfur dioxide (SO₂) and ash. SO₂ oxidizes to
57 sulfuric acid (H₂SO₄) which nucleates homogeneously or condenses on existing particles to form
58 sulfate aerosols (H₂SO₄-H₂O). Volcanic sulfate aerosols affect the Earth’s radiative balance by
59 increasing the scattering of incoming solar radiation and enhancing the infrared absorption
60 depending on the particle size, thus cooling the Earth’s surface and the troposphere, and warming

61 the stratosphere [*McCormick et al.*, 1995]. The influence of volcanic aerosols on stratospheric
62 ozone, particularly in the mid-latitudes, via heterogeneous chemistry is also well known, as
63 briefly discussed below.

64 Observational and modeling studies conducted after the Pinatubo volcanic eruptions
65 provided evidence of decreases in nitrogen oxides ($\text{NO}_x = \text{NO} + \text{NO}_2$) and increases in reactive
66 halogen radicals via heterogeneous chemistry on sulfate aerosols. As a result, the NO_x -catalyzed
67 ozone loss is suppressed, particularly in the middle stratosphere where the NO_x cycle is efficient
68 at destroying ozone [*Brasseur et al.*, 1999]. The reduction in NO_x also limits the formation of
69 reservoir species, such as chlorine nitrate (ClONO_2) and bromine nitrate (BrONO_2), increasing
70 the abundance of reactive halogen (ClO_x , BrO_x), and to a lesser extent, hydrogen oxides (HO_x).
71 Reactive halogen radicals are also enhanced due to heterogeneous activation on sulfate aerosols.
72 Thus, the efficiency of ozone destruction by ClO_x , BrO_x , and HO_x cycles [*Wennberg et al.*, 1994;
73 *Lary et al.*, 1996; *Solomon et al.*, 1996] is enhanced in the presence of volcanic sulfate aerosols
74 (see *Solomon* [1999] for a detailed review). The net impact of enhanced volcanic aerosols in the
75 present atmosphere is to increase ozone in the middle stratosphere and decrease ozone in the
76 lower stratosphere, resulting in a net decrease of ozone column. The overall effect on global
77 ozone burden has been shown to depend on the halogen loading of the atmosphere [*Tie and*
78 *Brasseur*, 1995; *Austin et al.*, 2013].

79 Multi-model projections of future ozone levels and the dates of ozone recovery to 1980
80 levels vary by latitude region and are dependent upon the assumed projection of well-mixed
81 greenhouse gases (WMGGs), including carbon dioxide (CO_2), methane (CH_4) and nitrous oxide
82 (N_2O), and ozone depleting substances (ODSs), and the resulting climate and stratospheric
83 circulation changes [*Pawson et al.*, 2014]. The possibility of significant changes in stratospheric

84 aerosol levels has been identified to be a key uncertainty in predicting future ozone abundance
85 by the World Meteorological Organization (WMO) and United Nations Environment Programme
86 (UNEP) Scientific Assessment of Ozone Depletion [Bekki *et al.*, 2011]. In this study, we perform
87 transient 21st century simulations with the U.S. NOAA Geophysical Fluid Dynamics Laboratory
88 (GFDL) fully interactive chemistry-climate model (GFDL-CM3) to assess ozone recovery in
89 response to the Representative Concentration Pathway (RCP) 4.5 and 8.5 climate forcing
90 scenarios under three different assumptions of stratospheric aerosol loading .

91

92 **2. Model and Simulations**

93 We employ the GFDL-CM3 chemistry-climate model [Donner *et al.*, 2011; John *et al.*,
94 2012; Austin *et al.* 2013; Westervelt *et al.*, 2015; Barnes *et al.*, 2016] in this study. Transient
95 historical (1860-2005) and future (2006-2100) simulations of CM3 were conducted in support of
96 the Coupled Model Intercomparison Project (CMIP5) and informed the Intergovernmental Panel
97 on Climate Change Assessment Report 5 (IPCC AR5). CM3 uses a finite-volume dynamical core
98 on a cubed-sphere horizontal grid composed of six faces, each with a horizontal domain of
99 48×48 grid cells, denoted as C48 horizontal resolution, and 48 vertical hybrid sigma-pressure
100 levels extending from the surface to 0.01 hPa (~80 km). The model simulates tropospheric and
101 stratospheric gas phase and heterogeneous photochemical processes over the full model domain
102 [Austin *et al.*, 2013; Naik *et al.*, 2013]; the simulated three dimensional ozone distribution
103 influences radiation calculations. Stratospheric chemistry includes gas-phase reactions describing
104 the HO_x, NO_x, ClO_x, and BrO_x catalytic cycles and heterogeneous reactions on solid nitric acid
105 trihydrate (NAT) and water-ice polar stratospheric particles, and liquid binary and ternary sulfate
106 polar stratospheric cloud (PSC) particles [Austin and Wilson, 2010]. Global mean tropospheric

107 volume mixing ratios of ozone depleting substances (ODSs) – including chlorofluorocarbons
108 (CFCs), hydrochlorofluorocarbons (HCFCs), halons, and bromine from very short-lived
109 substances (VSLS; shown to be important during periods of elevated aerosol surface area) – are
110 specified as a function of time providing a parametrized source of reactive halogens to the
111 stratosphere [Austin *et al.*, 2013].

112 Direct injection of aerosols or their precursors into the stratosphere is not considered
113 explicitly as the stratospheric aerosol life cycle is not represented in the model. Instead, the
114 radiative influence of stratospheric volcanic aerosols is accounted for by implementing vertically
115 resolved spatial and temporal distributions of aerosol optical properties (monthly mean aerosol
116 extinction, single scattering albedo, and asymmetry factor) following *Stenchikov et al.* [1998].
117 This dataset originally developed for the Pinatubo eruption based on satellite measurements by
118 *Stenchikov et al.* [1998] has been extended to cover the historical time period (1850-1999) based
119 on volcanic aerosol optical depths from *Sato et al.* [1993] and its updates. Volcanic aerosol
120 surface area density (SAD) is derived from aerosol extinction centered at 1.0- μm following the
121 relationship of *Thomason et al.* [1997], and is used for calculating heterogeneous reaction rates.

122 The historical CM3 simulations have been shown to generally reproduce well the
123 observed total ozone column over the past several decades, except for a high bias in the tropics
124 and southern mid-latitudes [Austin *et al.*, 2013]. The positive bias in the southern mid-latitudes is
125 likely due to excessive transport of ozone by the Brewer Dobson circulation from the tropics,
126 where ozone is already high, to the mid-latitudes [Austin *et al.*, 2013; Eyring *et al.*, 2013]. These
127 deficiencies in the model will most likely have minor impact on our results as our analysis
128 focuses on relative differences. Additionally, we evaluate the response of ozone to volcanic
129 aerosols by comparing monthly mean total ozone anomalies for the 5-year period encompassing

130 the Mt. Pinatubo eruption computed with historical CM3 simulations [Austin et al., 2013] against
131 observations [Frith et al., 2013; Bodeker et al., 2005] (Figure 1). The anomalies are calculated
132 relative to the mean over 1990-1999 period and the contributions due to quasi-biennial
133 oscillation (QBO), El Nino Southern Oscillation (ENSO), solar cycle, and changing stratospheric
134 chlorine and bromine have not been removed. Globally, the observations show a slow decline in
135 monthly total column ozone after Mt. Pinatubo eruption reaching a minimum of about -8 Dobson
136 Units (DU) in early 1993. The ensemble mean model is able to capture the observed variation in
137 global monthly column ozone, although it has some difficulty in reproducing the observed
138 minimum (Figure 1a). At least one ensemble member reproduces the observed global mean
139 ozone minimum. Additionally, a simulation of the atmospheric component of CM3 (AM3) with a
140 similar configuration as the historical CM3 simulations but nudged to NCEP-NCAR reanalysis
141 winds over the 1980-2012 period [Lin et al., 2014; 2015] is able to better match the observed
142 variations in global mean column ozone (blue lines on Figure 1a), suggesting that the response to
143 Pinatubo aerosols in the free-running CM3 is strongly influenced by dynamical variability and
144 feedbacks.

145 Despite depletion of stratospheric NO₂ in both the hemispheres after the Pinatubo
146 eruption [Pawson et al., 2014 and references therein], observations indicate an interhemispheric
147 asymmetry in the mid-latitude ozone response to Pinatubo aerosols with enhanced ozone loss in
148 the Northern Hemisphere (NH) mid-latitudes and a small increase of ozone column in the
149 Southern Hemisphere (SH) mid-latitudes [Randel et al., 1995]. Recent studies have attributed
150 this asymmetry to enhanced ozone transport in the SH that counterbalances the aerosol-induced
151 ozone loss [Poerberaj et al., 2011; Aquila et al., 2013; Dhomse et al., 2015]. Observations show
152 total column ozone decreases of up to 10 DU and 30 DU in December 1991 and January 1993,

153 respectively, in the NH mid-latitudes (Figure 1b), and about 10 DU increase after the eruption
154 from July to December 1991 and then a sharp decline reaching a minima of -10 DU in late 1992
155 in the SH mid-latitudes (Figure 1c). The mean model does not reproduce variations in NH mid-
156 latitudes, although at least one ensemble member is able to capture the column ozone decrease in
157 December 1991 (Figure 1b). In the SH mid-latitudes, the mean model is able to reproduce
158 variability to some extent but has difficulty in capturing the timing of the increase in ozone
159 column immediately after the eruption (Figure 1c). Discrepancies in chemistry-climate model
160 simulations of the interhemispheric asymmetry in the ozone response to Pinatubo have been a
161 problem [SPARC 2010, chapter 8]. Models forced with re-analyzed meteorological fields show
162 better skill in simulating the enhanced ozone loss in NH and the smaller ozone loss in SH
163 pointing to the importance of dynamical forcing on ozone changes [Shepherd *et al.*, 2014;
164 *Dhomse et al.*, 2015]. Indeed, the AM3 simulation nudged to NCEP-NCAR reanalysis winds
165 over the 1980-2012 period [Lin *et al.*, 2014; 2015] shows much better skill in reproducing the
166 observed interhemispheric asymmetry in the ozone response to Pinatubo aerosols (blue lines on
167 Figure 1b, c).

168 We analyze results from three-member ensembles of transient CM3 simulations for the
169 2006-2100 time period, with concentrations of WMGGs, ODSs, and short-lived species
170 emissions, following either the RCP 4.5 [Thomson *et al.*, 2011] or RCP 8.5 [Riahi *et al.*, 2011]
171 climate forcing scenarios (Table 1 and Figure 2). These ensemble members are initialized from
172 the respective members of the historical CM3 simulation [Austin *et al.*, 2013]. For each climate
173 forcing scenario, we consider three fixed levels of monthly-varying stratospheric aerosol loading
174 repeated over the 95 years of each simulation: background (BG) levels of sulfate aerosols during
175 non-volcanic periods (represented by values for year 1999) [Morgenstern *et al.*, 2010], periods of

176 weak volcanic activity (represented by year 1860), and moderate volcanic activity (represented
177 by the historical mean (HM) over the 1860-2000 period) (Table 1). The 1860 and historical mean
178 aerosol loadings are chosen arbitrarily from the volcanic aerosol dataset implemented in CM3
179 [Stenchikov *et al.*, 1998] to denote low and moderate volcanic aerosol loadings. The simulations
180 are denoted as RCPX.X_BG, RCPX.X_1860, and RCPX.X_HM, where X.X represents either
181 4.5 or 8.5.

182 The global annual mean volcanic aerosol optical depth (AOD) in the visible wavelength
183 (550 nm) in RCPX.X_BG, RCPX.X_1860, and RCPX.X_HM simulations is 0.0005, 0.0045, and
184 0.013, respectively. The volcanic AOD in RCPX.X_1860 is close to that observed for tropical
185 volcanic eruptions occurring in the 2000-2010 period, while that in RCPX.X_HM is similar to
186 AOD observed for the moderate volcanic events in the mid 1980s [Vernier *et al.* 2011]. Annual
187 average zonal mean volcanic aerosol SAD in the BG, 1860 and HM simulations are shown in
188 Figure 3.

189 For the analysis discussed below, we average results across ensemble members to better
190 isolate the forced response to volcanic aerosols. Stratospheric ozone column is defined here as
191 ozone concentrations integrated above 200 hPa. For each RCP scenario, we evaluate the impact
192 of increased volcanic aerosols by comparing the results for 1860 and HM simulations against
193 those of the corresponding BG simulation.

194

195 **3. Impact of Volcanic Aerosols on Stratospheric Ozone**

196 **3.1 Ozone Column**

197 We first analyze the long term evolution of stratospheric ozone column relative to 1980
198 levels in a manner consistent with previous multi-model projections [Eyering *et al.*, 2010b; 2013].

199 Figure 4 shows the 1980 baseline-adjusted time series of annual mean stratospheric ozone
200 column from 1960 to 2100, globally and averaged over five selected latitude bands. Results are
201 plotted for 1960-2005 from the historical simulations with time-varying stratospheric aerosols
202 [Austin *et al.*, 2013] and for 2006-2100 from the RCPX.X_* simulations discussed above. Values
203 are smoothed with a 1:2:1 filter applied 30 times iteratively [see Eyring *et al.*, 2010b; smoothing
204 was performed 50 times for polar region] to reduce interannual variability. In the 2000-2020
205 timeframe, stratospheric ozone column recovery in the RCPX.X_1860 simulations (blue lines) is
206 similar to that in the RCPX.X_BG simulations (black lines) but it is slower in the RCPX.X_HM
207 simulations (red lines; Figure 4a). After the mid-2020s, the adjusted stratospheric ozone columns
208 in both the RCPX.X_1860 and RCPX.X_HM simulations exceed the respective RCPX.X_BG
209 simulations and recover to 1980 levels earlier than in the RCPX.X_BG simulations. Global
210 stratospheric ozone column returns to 1980 levels in the RCP8.5_HM and RCP8.5_1860
211 simulations three to seven years earlier (2045-2049) than in the RCP8.5_BG simulation (2052),
212 while for the RCP4.5 scenario, return dates range from 2056 to 2071 compared to RCP4.5_BG in
213 which ozone remains below 1980 levels throughout the 21st century. By 2100, the global
214 stratospheric ozone column relative to 1980 levels is projected to range from 0.5-3 DU in the
215 RCP4.5 and 11-13 DU in the RCP8.5 simulations with 1860 and HM aerosol loading compared
216 to -2.6 and 9.3 DU in the RCP4.5_BG and RCP8.5_BG simulations, respectively. The response
217 of global mean stratospheric ozone column to elevated volcanic aerosols results from the
218 combination of different responses in the tropics, mid-latitudes, and polar regions as discussed
219 below.

220 In the tropics, the annual mean stratospheric ozone column does not recover to 1980
221 levels (Figure 4b) in any of the simulations; however, it is greater in RCPX.X_1860 and

222 RCPX.X_HM compared to the respective RCPX.X_BG simulations from about 2020 through
223 the end of the 21st century. Previous multi-model studies [Eyring *et al.*, 2010; 2013] attribute the
224 non-recovery of tropical stratospheric ozone column in simulations with increasing WMGGs and
225 declining ODSs to a combination of a) decreases in lower stratospheric ozone due to enhanced
226 tropical upwelling from WMGG-induced warming and b) increases in middle to upper
227 stratospheric ozone from WMGG-induced cooling that slows down ozone destruction. Elevated
228 volcanic aerosol loading in RCPX.X_1860 and RCPX.X_HM leads to warming of the tropical
229 lower stratosphere relative to RCPX.X_BG (not shown) due to the absorption of longwave
230 radiation, consistent with results of geoengineering model experiments in which stratospheric
231 sulfate aerosols are artificially enhanced [Tilmes *et al.*, 2009; Heckendorn *et al.*, 2009; Pitari *et*
232 *al.*, 2014]. This warming causes lower stratospheric ozone to decrease due to enhanced
233 upwelling of ozone-poor air through the end of the 21st century. In contrast, ozone increases in
234 the middle to upper tropical stratosphere in RCPX.X_1860 and RCPX.X_HM relative to
235 RCPX.X_BG due to the suppression of the NO_x-catalyzed ozone loss (discussed in the next
236 section). The net effect of these opposing ozone responses is that at 2100 the annual mean
237 tropical adjusted-stratospheric ozone column ranges from -7.9 to -6 DU in RCP4.5 and -4 to -5
238 DU in RCP8.5 simulations with 1860 and HM aerosol loading, a smaller decrease relative to
239 1980 values than the -9.2 and -6.0 DU found in the RCP4.5_BG and RCP8.5_BG simulations,
240 respectively.

241 In the mid-latitudes, the RCPX.X_1860 and RCPX.X_HM projections of the adjusted-
242 stratospheric ozone column (Figures 4c and 4d) evolve in a similar manner as that for the global
243 mean. The ozone return dates to 1980 values are significantly earlier in RCP4.5_1860 (2062) and
244 RCP4.5_HM (2046) than in the RCP4.5_BG simulation in the Northern Hemisphere mid-

245 latitudes but not in the Southern Hemisphere mid-latitudes. The ozone return dates are not
246 statistically significantly different in the RCP8.5_1860 and RCP8.5_HM relative to RCP8.5_BG
247 at either the northern or southern mid-latitudes. At 2100, the annual mean adjusted-stratospheric
248 ozone column in the northern mid-latitudes is 0, 3, and 7 DU for RCP4.5 and 19, 22, and 25 DU
249 for RCP8.5 with BG, 1860 and HM aerosol loadings, respectively. In southern mid-latitudes, the
250 adjusted-stratospheric the ozone column is 5, 10, and 12 DU for RCP4.5, and 24, 26, and 28 DU
251 for RCP8.5 with BG, 1860 and HM aerosol loadings, respectively. Figure 4 also shows that
252 ozone column in the mid-latitudes has greater sensitivity to the WMGG scenarios than in the
253 tropics. This likely results from a) stronger WMGG-induced stratospheric cooling that slows
254 down ozone loss rates in the upper stratosphere leading to enhanced ozone [e.g., *Eyring et al.*,
255 2010a,b; 2013], b) a factor of 2.5 higher methane concentration in RCP8.5 [*Meinshausen et al.*,
256 2011] leading to greater ozone increase in lower stratosphere and troposphere [*Revell et al.*,
257 2012; *Young et al.*, 2013], and c) greater WMGG-induced acceleration of Brewer-Dobson
258 circulation resulting in increased stratosphere-troposphere exchange and ozone flux, particularly
259 in the northern mid-latitudes [*Bekki et al.*, 2011; *Pawson et al.*, 2014].

260 The long-term evolution of stratospheric ozone column in the polar regions appears to be
261 insensitive to the volcanic aerosol loading (Figures 4e and 4f). Over the Arctic in March, ozone
262 recovery is mostly similar amongst the three aerosol loadings (BG, 1860 and HM) with similar
263 1980 return dates across the RCPs (Figure 1e). Post recovery, ozone column remains insensitive
264 to aerosol loadings but is sensitive to the RCP scenario as indicated by the ~ 40 DU difference
265 between RCP4.5 and RCP8.5 at 2100 attributed to the stronger effect of transport-induced
266 changes and chemical impacts in RCP8.5 consistent with previous studies [*Eyring et al.*, 2010b;
267 2013]. Over the Antarctic in October, ozone recovery is sensitive to neither volcanic aerosol

268 loadings nor the RCP scenarios considered here (Figure 4f) consistent with previous multi-model
269 projections [Eyring *et al.*, 2013].

270

271 3.2 Vertical Distribution of Zonal Mean Ozone Concentration

272 To decipher the trends in the stratospheric ozone columns, we analyze the difference in
273 the zonal mean ozone concentrations simulated for RCPX.X_1860 and RCPX.X_HM relative to
274 the respective RCPX.X_BG simulations for the mean 2006-2015 and 2091-2100 time periods. In
275 the 2006-2015 period (Figure 5, top) when stratospheric halogen loading is still sufficiently high
276 (Figure 2), annual mean ozone concentrations are simulated to increase in the middle
277 stratosphere and decrease in the lower stratosphere for RCPX.X_1860 and RCPX.X_HM relative
278 to the respective RCPX.X_BG. These differences are weaker for the RCPX.X_1860 simulations
279 with smaller volcanic aerosol loading compared to the RCPX.X_HM simulations with greater
280 aerosol loading. The zonal mean ozone differences are similar in the two RCPs ranging from -0.1
281 to +0.2 ppmv in the RCP4.5_1860 and RCP8.5_1860 simulations, and -0.14 to +0.4 ppmv in the
282 RCP4.5_HM and RCP8.5_HM simulations relative to the respective RCPX.X_BG. This
283 similarity in ozone response to volcanic aerosols between the two RCPs is driven by the
284 similarity in the WMGG and ODS projections in the early 21st century consistent with the
285 findings of Eyring *et al.* [2013].

286 In the 2091-2100 time period (Figure 5, bottom) when stratospheric halogen loading has
287 diminished significantly (but is still above the natural background), stronger increases in annual
288 mean ozone concentrations in the middle stratosphere and negligible decreases in the lower
289 stratosphere are simulated for RCPX.X_1860 and RCPX.X_HM relative to the respective
290 RCPX.X_BG. The importance of halogen chemistry has diminished over this time period as

291 evidenced by the absence of statistically significant differences in ozone in the lower stratosphere
292 where ozone decreased in response to volcanic aerosols for the 2006-2015 period (Figure 5).
293 This is consistent with the results of *Austin et al.* [2013] who found a temporary increase in
294 ozone column in response to volcanic eruptions in the pre-halogen era. Like the 2006-2015
295 period, ozone response to volcanic aerosols is stronger in the HM simulations with greater
296 aerosol loading. The increase in ozone from increasing volcanic aerosol loadings at 2091-2100 is
297 consistently weaker for RCP8.5 than that simulated for RCP4.5, reflecting the role of greater
298 methane loading in RCP8.5 which we discuss in the next section.

299

300 3.3 Chemical Partitioning versus Aerosol Surface Area Density

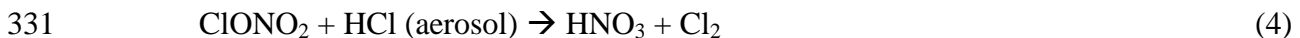
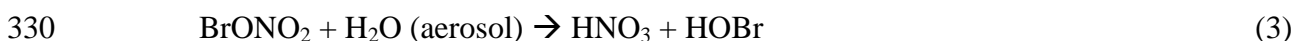
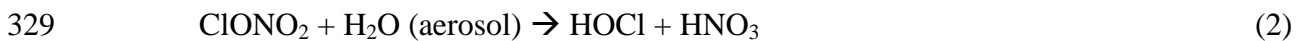
301 Next, we analyze the mechanisms of stratospheric ozone response by examining the
302 differences in chemical partitioning of reactive nitrogen (NO_y), reactive chlorine (Cl_y), and
303 reactive bromine (Br_y), as a function of volcanic SADs, focusing on the northern mid-latitudes.
304 At 50°N the simulated activated chlorine and bromine, measured as annual mean ClO/Cl_y and
305 BrO/Br_y ratios increase with increasing aerosol SAD while activated NO_x (NO_x/NO_y) decreases
306 in both RCP4.5 (Figures 6 a-e') and RCP8.5 (Figures 6 (f-j')) scenarios; ClO/Cl_y and BrO/Br_y
307 increase more strongly in the near term (2006-2015) when halogen loading is still high than in
308 the future, particularly in the upper (17hPa) stratosphere (Figures 6 a, e, f, j). Similar
309 dependencies are simulated for the southern mid-latitudes (not shown).

310 These differences in the partitioning of NO_y and halogens are attributed to heterogeneous
311 reactions occurring on stratospheric aerosol surfaces [see review of *Solomon* 1999]. The key
312 reaction linking volcanic aerosol changes to ozone depletion is the hydrolysis of N_2O_5 to nitric
313 acid (HNO_3) that depletes NO_x :



315 Due to enhanced hydrolysis of N_2O_5 to HNO_3 as volcanic aerosol SAD increases, NO_x is
316 depleted in RCPX.X_1860 and RCPX.X_HM relative to RCPX.X_BG resulting in lower
317 NO_x/NO_y (Figures 6 a, a', f, f') and higher HNO_3/NO_x (Figure 6 c, c', h, h'). This repartitioning
318 causes NO_x -catalyzed ozone loss to be suppressed at both the time periods. Since NO_x -induced
319 ozone loss is dominant in the middle stratosphere [*Brasseur et al.*, 1999], this is where ozone is
320 most enhanced in response to elevated volcanic aerosols (Figure 5).

321 Depleted NO_x not only reduces NO_x -catalyzed ozone loss but also perturbs halogen
322 partitioning, enhancing the ClO_x - and BrO_x -catalyzed ozone loss in the lower stratosphere where
323 these catalytic cycles dominate. Since less NO_2 is available to combine with ClO to produce the
324 reservoir species, ClONO_2 , more chlorine remains activated. Activated bromine is similarly
325 increased by reduced formation of BrONO_2 although to a lesser extent. Thus, ClO/Cl_y and
326 BrO/Br_y increase with increasing aerosol SADs, particularly in the 2006-2015 timeframe with
327 elevated halogen levels in the atmosphere (Figure 6). Additional heterogeneous reactions on
328 sulfate aerosols also increase halogen activation:



332 Typically, these occur on polar stratospheric clouds (solid NAT and water ice) in the extremely
333 cold polar stratosphere; however, with enhanced aerosol surface areas, these reactions can
334 proceed on liquid sulfate aerosols in the northern mid-latitudes due to temperature and water
335 vapor fluctuations [*Solomon*, 1999 and references therein].

336 Finally, gas-phase formation of HNO₃ via OH + NO₂ + M reaction competes with
337 reaction 1. Higher aerosol SAD leads to OH increases (not shown) that enhance the HO_x-
338 catalyzed ozone loss and increase the gas-phase conversion of hydrochloric acid (HCl) to
339 reactive chlorine [*Granier and Brasseur, 1992*] via:



341 Reactions 4 and 5 lead to decreases in HCl as evident from decreasing HCl/Cl_y with increasing
342 aerosol SAD in both the RCP4.5 (Figure d, d') and RCP8.5 simulations (Figure 6 i, i').

343 For RCP4.5, the HNO₃/NO_x ratio is similar over the 2006-2015 and 2091-2100 time
344 periods (Figure 6 c, c'), but for RCP8.5 the HNO₃/NO_x ratio increases significantly between the
345 two periods (Figure 6 h, h') due to the increased OH from the higher water vapor driven by a
346 factor of 2.5 methane increase projected for RCP8.5 (as opposed to a small decrease for RCP4.5;
347 see Figure 2). The increased OH in RCP8.5 increases the gas-phase production of HNO₃, thus
348 making the chemistry less sensitive to aerosol SAD increases as evident from the gradual change
349 in the NO_x/NO_y ratio with increasing SAD at 2091-2100 (Figure 6 g, g'). This leads to a weaker
350 ozone enhancement in RCP8.5 from elevated volcanic aerosols as compared to that in RCP4.5 at
351 2091-2100 (Figure 5).

352 The net effect on ozone of changes in Cl_y, Br_y, and NO_y partitioning in response to
353 volcanic aerosols is thus a balance between competing effects on NO_x-, HO_x- and halogen-
354 catalyzed ozone loss cycles, with the net impact depending on the altitude, atmospheric halogen
355 (and methane) loading, and volcanic aerosol loading. For the range of aerosol loadings
356 considered here, the ozone response to volcanic aerosols does not saturate as suggested by
357 *Prather et al. [1992]*.

358

359 4. Conclusions and Discussion

360 Analyses of transient three-member ensemble simulations of GFDL CM3 following two
361 climate scenarios (RCP4.5 and RCP8.5) indicate that stratospheric ozone exhibits opposing
362 changes in response to elevated volcanic aerosols at different altitudes and halogen levels. In the
363 early 21st century, increased halogen-catalyzed ozone loss in the lower stratosphere offsets the
364 suppressed NO_x-catalyzed ozone loss in the middle stratosphere, resulting in largely similar
365 recovery of global mean stratospheric ozone column in RCPX.X_1860 and RCPX.X_BG
366 simulations; the RCPX.X_HM simulations with greater volcanic aerosols exhibit slow ozone
367 column recovery during this period due to the greater activation of halogen radicals causing
368 increased ozone loss. After about the mid-2020s, when halogen levels have diminished (but are
369 still above the natural background), the NO_x suppression by volcanic aerosols dominates, leading
370 to stronger stratospheric ozone recovery in scenarios with elevated volcanic aerosols. Ozone
371 column returns to 1980 levels in the mid-2040s in RCP8.5_1860 and RCP8.5_HM simulations
372 (three to seven years earlier than in RCP8.5_BG), while its recovery date ranges from mid 2050s
373 to early 2070s in the RCP4.5_1860 and RCP4.5_HM simulations compared to RCP4.5_BG in
374 which it remains below 1980 levels through 2100. These results are sensitive to the amount of
375 aerosol loading, as indicated by weaker responses in RCPX.X_1860 compared to those in
376 RCPX.X_HM simulations. Further, stratospheric ozone recovery by year 2100 in simulations
377 with elevated volcanic aerosols relative to background is greater in RCP4.5 versus RCP8.5 due
378 to a factor of 2.5 greater methane in RCP8.5 compared to RCP4.5.

379 The long-term evolution of stratospheric ozone column in response to different future
380 emissions scenarios varies by different latitude regions [e.g., *Eyring et al.*, 2013]; elevated
381 volcanic aerosols in the future act to enhance this variability. In the tropics, stratospheric ozone

382 column does not respond to elevated aerosols until about 2020, but thereafter is enhanced by
383 elevated volcanic aerosols in both RCP scenarios, although it remains below 1980 levels in all
384 simulations. In the mid-latitudes, stratospheric ozone column shows more sensitivity to elevated
385 volcanic aerosols in the Northern Hemisphere than in the Southern Hemisphere. The sensitivity
386 is generally greater in RCP4.5 than in the RCP8.5 emission scenario. Over the polar regions, the
387 long term evolution of stratospheric ozone column is insensitive to the amount of volcanic
388 aerosol loading relative to the background, but Arctic ozone column is sensitive to the
389 greenhouse gas scenario.

390 Our findings are generally consistent with those of previous modeling studies that have
391 analyzed the impact of volcanic aerosols [*Granier and Brasseur, 1992; Tie and Brasseur, 1995;*
392 *Solomon et al., 1996; Austin et al., 2013; Aquila et al., 2013*] and the impact of geoengineering
393 via sulfate aerosols [*Heckendorn et al., 2009; Tilmes et al., 2009; Pitari et al., 2014*] on
394 stratospheric ozone in the presence of varying amounts of halogens following different WMGG
395 scenarios. Our simulated ozone response in RCP4.5_HM can be directly compared with those
396 simulated in multi-model geoengineering experiments conducted by imposing a constant sulfate
397 aerosol surface area increase similar to that produced following the Pinatubo eruption in the
398 RCP4.5 reference scenario [*Pitari et al., 2014*]. *Pitari et al.* find that increased aerosols would
399 cause global ozone column to decrease in the 2040-2049 decade relative to the base RCP4.5
400 scenario but to increase after 2050, similar to RCP4.5_HM results, although the timing of the
401 ozone response is somewhat different. *Pitari et al.* also find a net reduction of 5% in polar ozone
402 from elevated sulfate aerosols resulting from enhanced PSC formation, consistent with the
403 results of a more recent study in which an imposed factor of three enhancement in stratospheric
404 sulfate over 2011 levels increased ozone loss by up to 20 DU in the Antarctic and 15 DU in the

405 Arctic [Solomon *et al.*, 2015]. This conflicts with our result that polar stratospheric ozone
406 column appears to be insensitive to the amount of volcanic aerosol loading, especially in the
407 2006-2020 period when halogen levels are still high. Differences in the simulated polar
408 temperatures, chemical reaction rates, aerosol SAD, and halogen levels could potentially explain
409 some of this discrepancy over the polar regions. .

410 As with any modeling study, our results are subject to errors resulting from model
411 deficiencies. Model biases in the ozone and atmospheric circulation response to volcanic
412 aerosols and other forcing agents (e.g., WMGGs, ODSs) will likely affect our results. For
413 example, the better simulation of ozone response to Pinatubo aerosols by the nudged AM3
414 simulation compared to the free-running CM3 simulations demonstrates the influence of biases
415 in atmospheric circulation. The stratospheric halogen source is treated in a simplified manner in
416 our model to reduce computational cost; simulated Cl_y and Br_y have been shown to agree
417 generally with existing observations but have some discrepancies, particularly in the tropics
418 [Austin and Wilson, 2010], which may affect our results. CM3 does not explicitly simulate the
419 emission of stratospheric aerosol precursors, aerosol formation, transport, growth and loss
420 processes after volcanic eruptions – processes that determine the aerosol SAD distribution and
421 therefore affect the rate of heterogeneous reactions. Similar experiments with other global
422 models that include these processes will help provide more robust estimates of the influence of
423 stratospheric volcanic aerosols on ozone recovery. Further, our results are specific to the
424 idealized experiments conducted here, with imposed fixed levels of volcanic aerosols through the
425 21st century. In reality, stratospheric volcanic aerosol loadings will fluctuate, causing the timing
426 and extent of ozone recovery to vary correspondingly. It would be worth exploring the influence
427 of variable volcanic eruptions in the 21st century on the long term evolution of stratospheric

428 ozone. Finally, idealized volcanic-perturbation experiments conducted in support of Model
429 Intercomparison Project on the climatic response to Volcanic forcing (VolMIP) [Zanchettin *et al.*,
430 2016] can help assess the robustness of the stratospheric ozone response to strong volcanic
431 forcings simulated across chemistry-climate models and can help identify the causes of
432 differences in these responses.

433 Uncertainties in ozone projections and expected recovery dates have been recognized to
434 come from uncertainties in assumed ODS and WMGG emission scenarios, interannual
435 variability of ozone column, and diversity in model projections [Eyring *et al.*, 2013]. We show
436 here that volcanic aerosol perturbations also contribute to this uncertainty, thus providing a
437 knowledge base to interpret ozone results from future multi-model projections with volcanic
438 forcing prescribed to be equal to a constant historical mean value [O'Neill *et al.*, 2016]. The
439 novelty of our study lies in the use of transient simulations to 2100 using a state-of-the-art
440 chemistry-climate model to demonstrate that the influence of volcanic aerosols on the extent and
441 timing of the ozone recovery varies with: a) greenhouse gas scenarios, and b) halogen loading.
442 We have also highlighted the need to explore further the influence of increased methane
443 concentrations on stratospheric ozone column under conditions of elevated volcanic aerosols.

444 Predicting the timing and magnitude of volcanic eruptions on a global scale several
445 decades into the future is currently impossible. Model simulations that consider hypothetical
446 volcanic aerosol distributions based on recent measurements could help provide a lower limit of
447 the influence of volcanic aerosols on stratospheric ozone. The response of stratospheric ozone
448 column to observed SAD over the 2000-2014 period for which we now have observational
449 constraints [Kremser *et al.*, 2016 and references therein] can help provide estimates of the net
450 effect of recent observed SAD on stratospheric ozone column.

451

452 **Acknowledgments**

453 We are grateful to David Paynter and John Wilson for helpful discussions. We thank Pu Lin, Ron
454 Stouffer and two anonymous reviewers for helpful suggestions on an earlier version of the
455 manuscript. We also thank Greg Bodeker for providing access to the NIWA-BS total column
456 ozone database and acknowledge the NOAA SBUV data team for free access to their dataset. All
457 data used in this study can be obtained from the corresponding author (Vaishali.Naik@noaa.gov).

458

459 **References**

- 460 Aquila, V., L. D. Oman, R. Stolarski, A. R. Douglass, and P. A. Newman (2013), *J. Atmos. Sci.*,
461 **70**, 894-900, doi:10.1175/JAS-D-12-0143.1.
- 462 Austin, J., L. W. Horowitz, M. D. Schwarzkopf, R. J. Wilson, and H. Levy II (2013),
463 Stratospheric ozone and temperature simulated from the preindustrial era to the present day,
464 *J. Climate*, **26**, 3528-3542, doi:10.1175/JCLI-D-12-00162.1.
- 465 Austin, J. and R. J. Wilson (2010), Sensitivity of polar ozone to sea surface temperatures and
466 halogen amounts, *J. Geophys. Res.*, **115**, D18303, doi:10.1029/2009JD013292.
- 467 Barnes, E. A., A. M. Fiore, and L. W. Horowitz (2016), Detection of trends in surface ozone in
468 the presence of climate variability, *J. Geophys. Res. Atmos.*, **121**, 6112–6129,
469 doi:10.1002/2015JD024397.
- 470 Bekki et al. (2011), Future ozone and its impact on surface UV, Chapter 3 in *Scientific*
471 *Assessment of Ozone Depletion: 2010*, Global Ozone Research and Monitoring Project –
472 Report No. 52, 516pp., World Meteorological Organization, Geneva, Switzerland.

473 Bodeker, G. E., H. Shiona, and H. Eskes, (2005), Indicators of Antarctic ozone depletion, *Atmos.*
474 *Chem. Phys.*, **5**, 2603–2615, doi:10.5194/acp-5-2603-2005, 2005.

475 Brasseur, G. P., et al. (1999), *Atmospheric Chemistry and Global Change*, Oxford University
476 Press Inc., NY, USA.

477 Collins, M., et al. (2013), Long-term Climate Change: Projections, Commitments and
478 Irreversibility, in: *Climate Change 2013: The Physical Science Basis. Contribution of*
479 *Working Group I to the Fifth Assessment Report of the Intergovernmental Panel on Climate*
480 *Change* [Stocker, T. F., et al. (eds.)]. Cambridge University Press, Cambridge, United
481 Kingdom and New York, NY, USA.

482 Dhomse, S. S., M. P. Chipperfield, W. Feng, R. Hossaini, G. W. Mann, and M. L. Santee (2015),
483 Revisiting the hemispheric asymmetry in midlatitude ozone changes following the Mount
484 Pinatubo eruption: A 3-D model study. *Geophys. Res. Lett.*, **42**, 3038–3047. doi:
485 10.1002/2015GL063052.

486 Donner, L. J., et al. (2011), The dynamical core, physical parameterizations, and basic simulation
487 characteristics of the atmospheric component of AM3 of the GFDL global coupled model
488 CM3, *J. Climate*, **24**, 3484-3519.

489 Eyring, V., et al. (2010a), Multi-model assessment of stratospheric ozone return dates and ozone
490 recovery in CCMVal-2 models, *Atmos. Chem. Phys.*, **10**, 9451-9472, doi:10.5194/acp-10-
491 9451-2010.

492 Eyring, V., et al. (2010b), Sensitivity of 21st century stratospheric ozone to greenhouse gas
493 scenarios, *Geophys. Res. Lett.*, **37**, L16807, doi:10.1029/2010GL044443. Eyring, V., et al.
494 (2013), Long-term ozone changes and associated climate impacts in CMIP5 simulations, *J.*
495 *Geophys. Res.*, **118**, 1-32, doi:10.1002/jgrd.50316.

496 Fahey, D. W., et al. (1993), In situ measurements constraining the role of sulphate aerosols in
497 mid-latitude ozone depletion, *Nature*, 363, 509-514.

498 Frith, S. M., et al. (2013), Multi-satellite merged ozone (O3) profile and total column monthly
499 L3 global 5.0deg Lat Zones, version 1, Greenbelt, MD, USA:NASA Goddard Earth Science
500 Data and Information Services Center (GES DISC).

501 Granier, C., and G. Brasseur (1992), Impact of heterogeneous chemistry on model predictions of
502 ozone changes, *J. Geophys. Res.*, **97**(D16), 18015–18033, doi:10.1029/92JD02021.

503 Heckendorn, P., et al. (2009), The impact of geoengineering aerosols on stratospheric
504 temperature and ozone, *Environ. Res. Lett.*, **4**, doi:10.1088/1748-9326/4/4/045108.

505 Hofmann, D., J. Barnes, M. O'Neill, M. Trudeau, and R. Neely (2009), Increase in background
506 stratospheric aerosol observed with lidar at Mauna Loa Observatory and Boulder, Colorado,
507 *Geophys. Res. Lett.*, **36**, L15808, doi:10.1029/2009GL039008.

508 John, J., A. M. Fiore, V. Naik, L. W. Horowitz, and J. Dunne (2012), Climate versus emission
509 drivers of methane lifetime from 1860 to 2100, *Atmos. Chem. Phys.*, **12**, 12021-12036,
510 doi:10.5194/acp-12-12021-2012.

511 Junge, E., C. W. Chagnon, and J. E. Manson (1961), A world-wide stratospheric aerosol layer,
512 *Science*, **133**, 1478–1479, doi:10.1126/science.133.3463.1478-a.

513 Kremser, S., et al. (2016), Stratospheric aerosol – Observations, processes, and impact on
514 climate, *Rev. Geophys.*, doi: 10.1002/2015RG000511.

515 Lary, D. J., M. P. Chipperfield, R. Toumi, and T. Lenton (1996), Heterogeneous atmospheric
516 bromine chemistry, *J. Geophys. Res.*, **101**, 1489-1504.

517 Lin, M., L. W. Horowitz, S. J. Oltmans, A. M. Fiore, and S. Fan (2014), Tropospheric ozone
518 trends at Mauna Loa Observatory tied to decadal climate variability, *Nat. Geosci.*, **7**, 136–
519 143, 2014.

520 Lin, M., A. M. Fiore, L. W. Horowitz, A. O. Langford, S. J. Oltmans, D. Tarasick, and H. E.
521 Rieder (2015), Climate variability modulates western US ozone air quality in spring via deep
522 stratospheric intrusions, *Nat. Commun.*, **6**, 7105, doi:10.1038/ncomms8105.

523 McCormick, P. M., L. W. Thomason, and C. Trepte (1995), Atmospheric effects of the Mt.
524 Pinatubo eruption, *Nature*, **373**, 399–404, doi:10.1038/373399a0.

525 Meinshausen, M., et al. (2011), The RCP greenhouse gas concentrations and their extension from
526 1765 to 2300, *Clim. Change* (Special Issue), doi:10.1007/s10584-011-0156-z.

527 Morgenstern, O., et al. (2010), A review of CCMVal-2 models and simulations, *J. Geophys. Res.*,
528 **115**, D00M02, doi:10.1029/2009JD013728.

529 Naik, V., et al. (2013), Impact of preindustrial to present-day changes in short-lived pollutant
530 emissions on atmospheric composition and climate forcing, *J. Geophys. Res.*, **118**, 8086–
531 8110, doi:10.1002/jgrd.50608.

532 O'Neill, B. C., et al. (2016), The Scenario Model Intercomparison Project (ScenarioMIP) for
533 CMIP6, *Geosci. Model Dev. Discuss.*, doi:10.5194/gmd-2016-84, in review.

534 Pawson, S., et al. (2014), Update on global ozone: Past, present, and future, Chapter 2 in:
535 Scientific Assessment of Ozone Depletion: 2014, Global Ozone Research and Monitoring
536 Project – Report No. 55, World Meteorological Organization, Geneva, Switzerland, 2014.

537 Pitari, G., V. Aquila, B. Kravitz, A. Robock, S. Watanabe, I. Cionni, N. De Luca, G. Di Genova,
538 E. Mancini, and S. Tilmes (2014), Stratospheric ozone response to sulfate geoengineering:

539 Results from the Geoengineering Model Intercomparison Project (GeoMIP), *J. Geophys.*
540 *Res.*, **119**, 2629–2653, doi:10.1002/2013JD020566.

541 Poberaj, C. S., J. Staehelin, and D. Brunner (2011), Missing Stratospheric Ozone Decrease at
542 Southern Hemisphere Middle Latitudes after Mt. Pinatubo: A Dynamical Perspective, *J.*
543 *Clim.*, <http://dx.doi.org/10.1175/JAS-D-10-05004.1>.

544 Prather, M. (1992), Catastrophic loss of stratospheric ozone in dense volcanic clouds, *J.*
545 *Geophys. Res.*, **97**, 10187–10191, doi:10.1029/92JD00845.

546 Randall, W. J., J. M. Russell III, J. W. Waters, and L. Froidevaux, (1995), Ozone and temperature
547 changes in the stratosphere following the eruption of Mount Pinatubo, *J. Geophys. Res.*,
548 **100**(D8), 16,753-16,764.

549 Revell, L. E., G. E. Bodeker, P. E. Huck, B. E. Williamson, and E. Rozanov, (2012), The
550 sensitivity of stratospheric ozone changes through the 21st century to N₂O and CH₄, *Atmos.*
551 *Chem. Phys.*, **12**, 11309-11317, doi:10.5194/acp-12-11309-2012.

552 Riahi, K. et al. (2011), RCP8.5 – A scenario of comparatively high greenhouse gas emissions,
553 *Clim. Change.*, **109**, 33-57, 10.1007/s10584-011-0149-y.

554 Sato, M., J. E. Hansen, M. P. McCormick, and J. B. Pollack (1993), Stratospheric aerosol optical
555 depths, 1850–1990, *J. Geophys. Res.*, **98**, 22987–22994.

556 Shepherd, T., D. A. Plummer, J. F. Scinocca, M. I. Hegglin, V. E. Fioletov, M. C. Reader, E.
557 Remsberg, T. von Clarmann and H. J. Wang, (2015), Reconciliation of halogen-induced
558 ozone loss with the total-column ozone record, *Nat. Geosci.*, **7**, 443–449,
559 doi:10.1038/ngeo2155.

560 Solomon, S., R. W. Portmann, R. R. Garcia, L. W. Thomason, L. R. Poole, and M. P. McCormick
561 (1996), The role of aerosol variations in anthropogenic ozone depletion at northern mid-
562 latitudes, *J. Geophys. Res.*, **101**, 6713–6727, doi:10.1029/95JD03353.

563 Solomon, S. (1999), Stratospheric ozone depletion: A review of concepts and history, *Rev.*
564 *Geophys.*, **37**, 275–316, doi:10.1029/1999RG900008.

565 Solomon, S., D. Kinnison, J. Bandoro, and R. Garcia (2015), Simulation of polar ozone
566 depletion: An update. *J. Geophys. Res. Atmos.*, **120**, 7958–7974. doi:
567 10.1002/2015JD023365.

568 SPARC, 2006: SPARC Assessment of Stratospheric Aerosol Properties (ASAP). L. Thomason
569 and Th. Peter (Eds.), SPARC Report No. 4, WCRP-124, WMO/TD - No. 1295, available at
570 www.sparc-climate.org/publications/sparc-reports/

571 SPARC, 2010: SPARC CCMVal Report on the Evaluation of Chemistry-Climate Models

572 Stenchikov, G. L., I. Kirchner, A. Robock, H.-F. Graf, J. C. Antuna, R. G. Grainger, A. Lambert,
573 and L. Thomason (1998), Radiative forcing from the 1991 Mount Pinatubo volcanic
574 eruption, *J. Geophys. Res.*, **103**, 13,837–13,858, doi:10.1029/98JD00693.

575 Tilmes, S., R. R. Garcia, D. E. Kinnison, A. Gettelman, and P. J. Rasch (2009), Impact of
576 geoengineered aerosols on the troposphere and stratosphere, *J. Geophys. Res.*, **114**, D12305,
577 doi:10.1029/2008JD011420.

578 Thomason, L. W., L. R. Poole, and T. Deshler (1997), A global climatology of stratospheric
579 aerosol surface area density deduced from Stratospheric Aerosol and Gas Experiment II
580 measurements: 1984–1994, *J. Geophys. Res.*, **102**, 8967–8976, doi:10.1029/96JD02962.

581 Thomson, A. M., et al. (2011), RCP4.5: a pathway for stabilization of radiative forcing by 2100,
582 *Clim. Change*, 109, 77–94, doi:10.1016/s10584-011-0151-4.

583 Tie, X. X., and G. P. Brasseur (1995), The response of stratospheric ozone to volcanic eruptions:
584 sensitivity to atmospheric chlorine loading, *Geophys. Res. Lett.*, **22**, 3035-3038, doi:
585 10.1029/95GL03057.

586 Vernier, J. P., et al. (2009), Tropical stratospheric aerosol layer from CALIPSO lidar
587 observations, *J. Geophys. Res.*, **114**, D00H10, doi:10.1029/2009JD011946.

588 Vernier, J.-P., et al. (2011), Major influence of tropical volcanic eruptions on the stratospheric
589 aerosol layer during the last decade, *Geophys. Res. Lett.*, **38**, L12807,
590 doi:10.1029/2011GL047563.

591 Wennberg, P. O., et al. (1994), Removal of stratospheric ozone by radicals: In situ measurements
592 of OH, HO₂, NO, NO₂, ClO, and BrO, *Science*, 266, 398-404.

593 Westervelt, D .M., L.W. Horowitz, V. Naik, and D. L. Mauzerall (2015), Radiative forcing and
594 climate response to projected 21st century aerosol decreases, *Atmos. Chem. Phys.*, **15**, 12681-
595 12703, doi:10.5194/acp-15-12681.

596 Young, P. J., et al. (2013), Pre-industrial to end 21st century projections of tropospheric ozone
597 from the Atmospheric Chemistry and Climate Model Intercomparison Project (ACCMIP),
598 *Atmos. Chem. Phys.*, **13**, 2,063–2,090, doi:10.5194/acp-13-2063-2013.

599 Zanchettin, D., et al., (2016), The Model Intercomparison Project on the climatic response to
600 Volcanic forcing (VolMIP): experimental design and forcing input data for CMIP6, *Geosci.*
601 *Model Dev.*, **9**, 2701-2719, doi:10.5194/gmd-9-2701-2016.

602

603 **Tables**

604

605 **Table 1:** Overview of GFDL-CM3 three-member ensemble simulations conducted to assess the
606 influence of elevated volcanic aerosols on stratospheric ozone recovery.

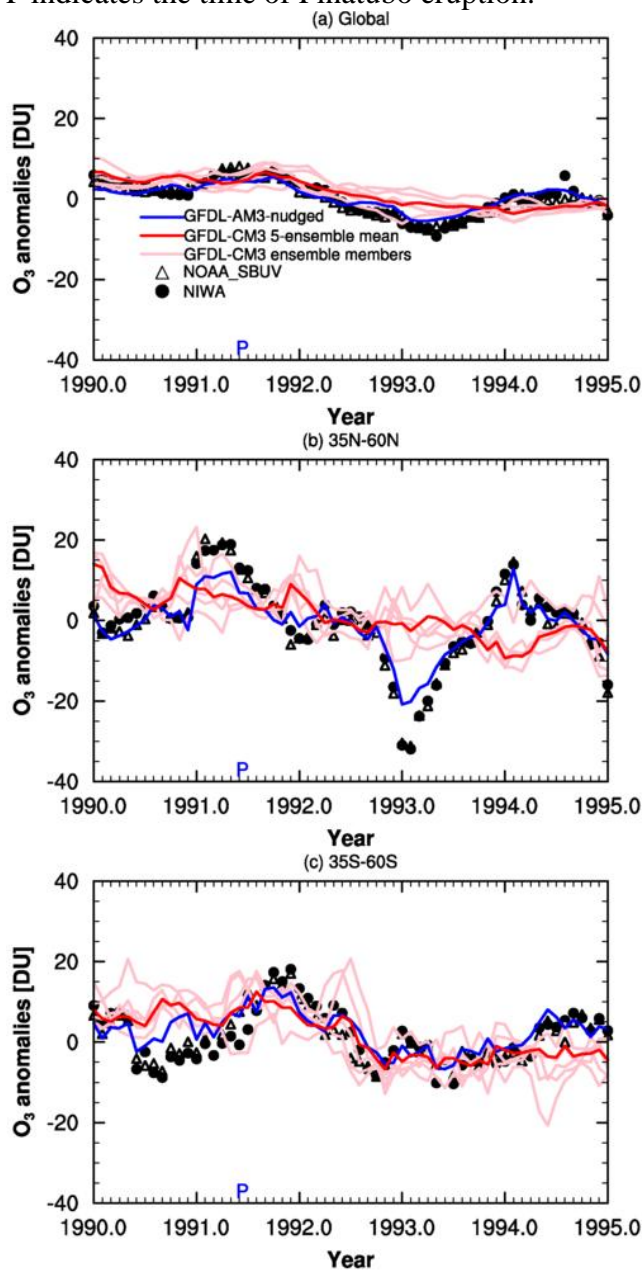
607

Experiment	Volcanic aerosol surface area density (SAD)	Greenhouse gases (CO ₂ , CH ₄ , N ₂ O) and Ozone Depleting Substances (ODSs)
RCP4.5_BG	1999	RCP4.5
RCP4.5_1860	1860	RCP4.5
RCP4.5_HM	Mean 1860-1999	RCP4.5
RCP8.5_BG	1999	RCP8.5
RCP8.5_1860	1860	RCP8.5
RCP8.5_HM	Mean 1860-1999	RCP8.5

608

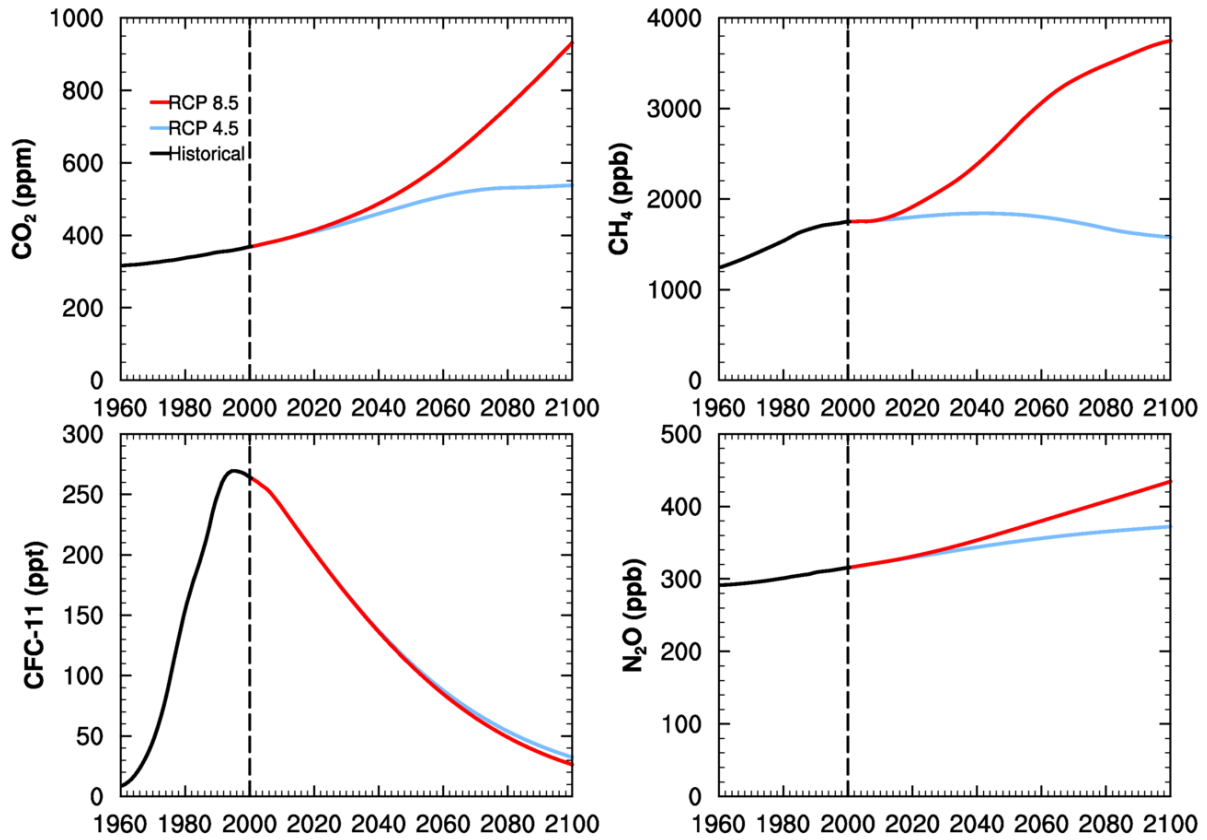
609 **Figures**

610 **Figure 1.** Total column ozone monthly mean anomalies [DU] from two observational datasets
611 and model simulations for a) global, (b) NH and (c) SH mid-latitudes. Anomalies were calculated
612 relative to monthly mean total column ozone averaged over 1990-1999 period. Observed
613 monthly average total ozone columns are taken from version 8.6 Solar Backscattered Ultra Violet
614 (SBUV) data from the Nimbus-4 BUUV, Nimbus-7 SBUV, and NOAA-9 through 18 SBUV/2
615 instruments [Frith *et al.*, 2013] (NOAA_SBUV) and version 2.8 of the monthly total column
616 ozone from NIWA-BS total column ozone (TCO) database [Bodeker *et al.*, 2005]. Blue-colored
617 P indicates the time of Pinatubo eruption.



618

619 **Figure 2.** Timeseries of carbon dioxide (CO₂), methane (CH₄), trichlorofluoromethane (CFC-11)
620 and nitrous oxide (N₂O) implemented in the simulations described in Table 1. Original data are
621 from Meinshausen et al. (2011).

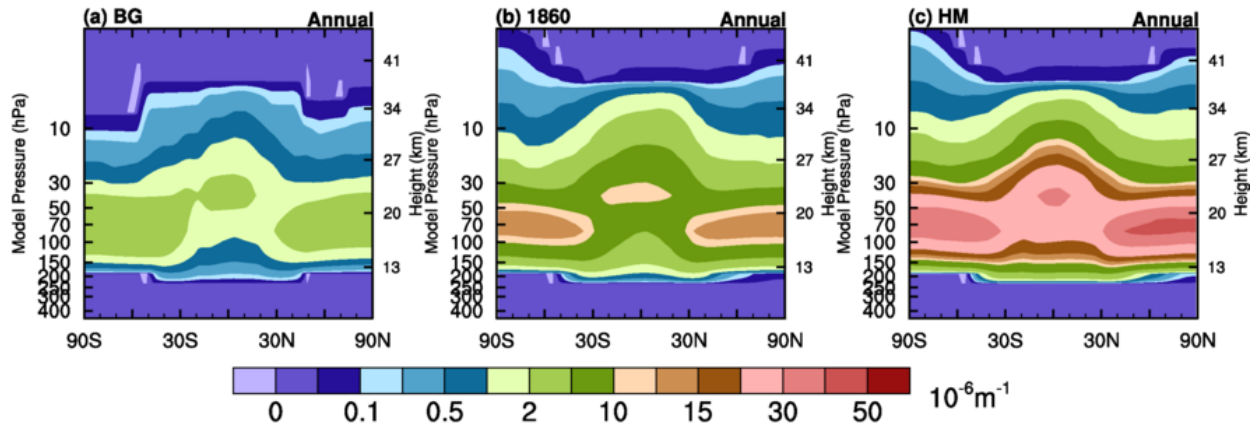


622

623

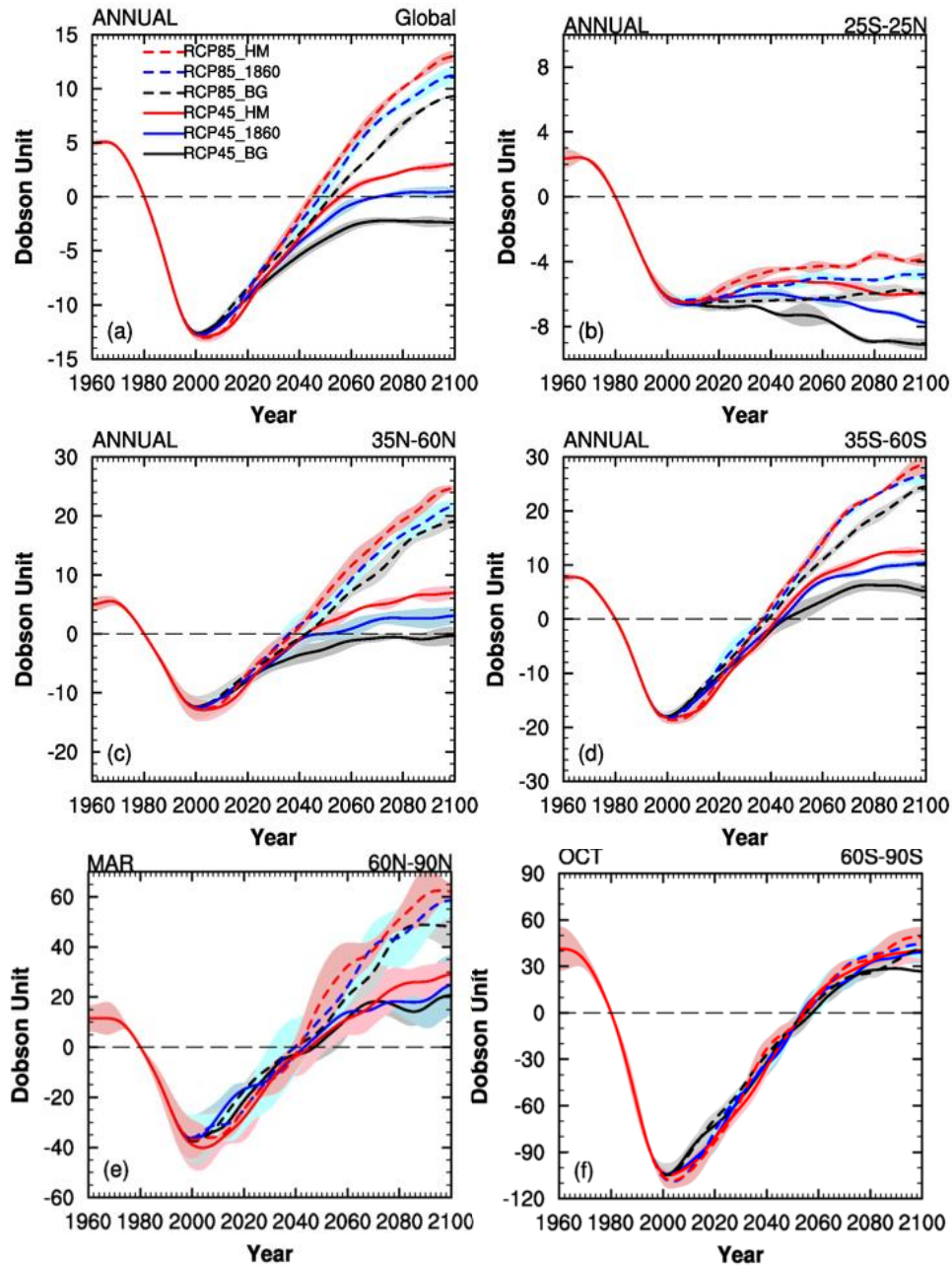
624

625 **Figure 3.** Annual mean zonal average volcanic aerosol surface area density implemented in the
626 (a) RCPX.X_BG, (b) RCPX.X_1860, and (c) RCPX.X_HM simulations.
627



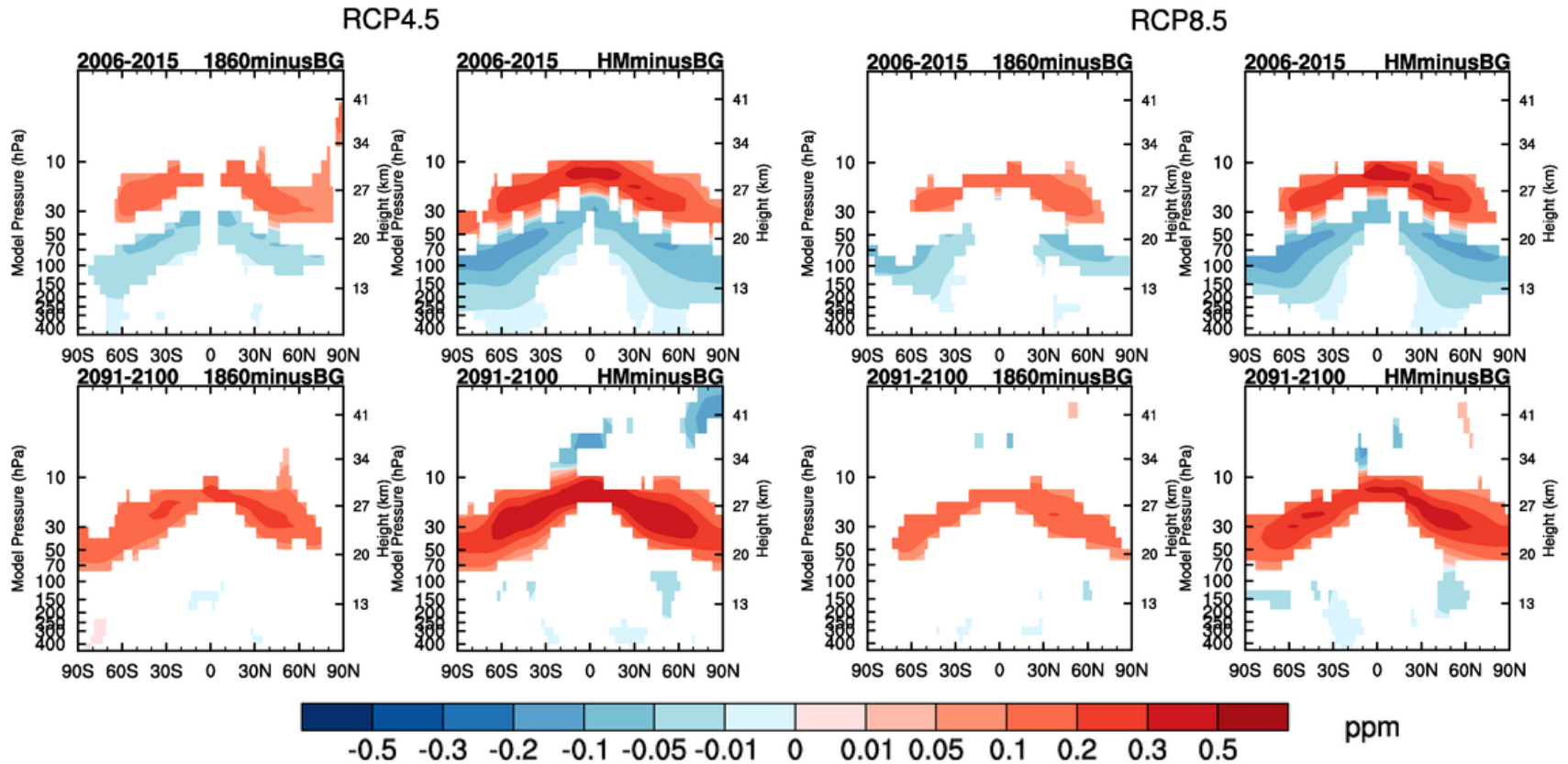
628
629

630 Figure 4. The 1980 baseline-adjusted time series of stratospheric ozone column (200 – 0 hPa)
 631 from 1960 to 2100 for the background (BG), 1860, and historical mean (HM) volcanic aerosols
 632 considered in RCP4.5 and RCP8.5 simulations. The panels show (a) global and annual average,
 633 (b) annual average over 25°N-25°S (c) annual average over 35°-60°N (d) annual average over
 634 35-60°S (e) averaged over 60-90°N for March, and (f) averaged over 60-90°S for October.
 635 Shaded areas indicate ± 1 -standard deviation across the three ensemble members for each
 636 simulation.

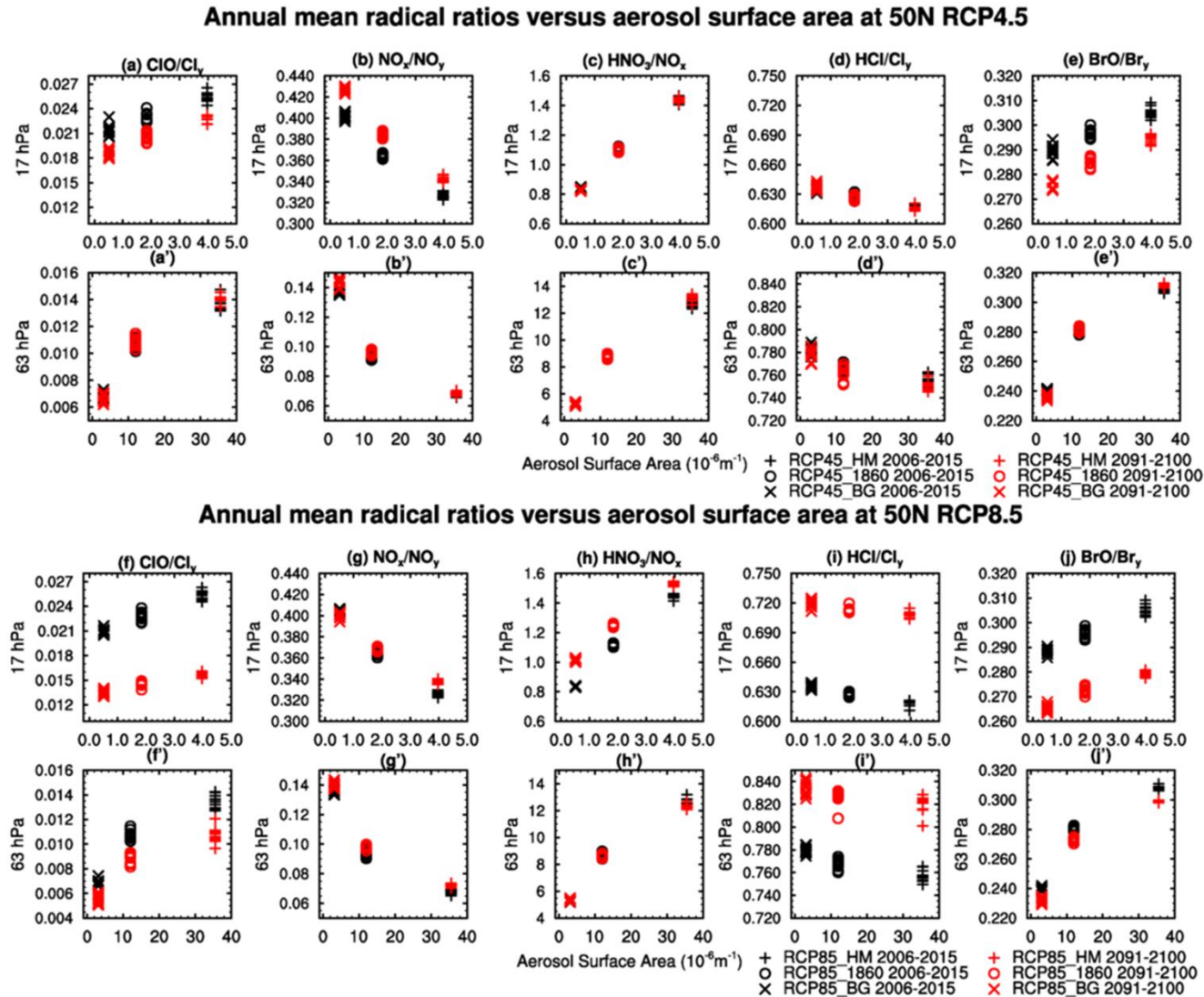


674 Figure 5. Difference in annual average zonal mean ozone concentration in RCP4.5 (left) and RCP8.5 (right) with 1860 and historical
675 mean (HM) volcanic aerosols relative background (BG) volcanic conditions. Top and bottom rows show differences for mean 2006-
676 2015 and 2091-2100 time periods, respectively. Only differences significant at 95% confidence level based on student's t-test are
677 shown.

678
679
680
681
682
683
684
685
686
687
688
689
690
691
692
693
694
695
696
697
698
699
700
701
702
703



704 Figure 6. Annual mean radical ratios as a function of volcanic aerosol surface area density (SAD) for 17hPa and 63hPa at 50°N.
 705 Values are individual years within 2006-2015 and 2091-2100 time periods averaged over three ensemble members of the
 706 RCPX.X_BG, RCPX.X_1860 and RCPX.X_HM simulations, where X.X = 4.5 (top) and 8.5 (bottom).
 707



708